Engineering the Next Generation of Solid State Proton Conductors: Synthesis and Properties of Ba$_{3-x}$K$_x$H$_x$(PO$_4$)$_2$[†]

Calum R.I. Chisholm,*,[‡] Eric S. Toberer,[‡] Mary W. Louie,[§] and Sossina M. Haile[‡,§]

[‡]*Materials Science 309-81, California Institute of Technology, Pasadena, California 91125 and* [§]*Chemical Engineering 210-41, California Institute of Technology, Pasadena, California 91125*

A new series of compounds with general chemical formula Ba$_{3-x}$K$_x$H$_x$(PO$_4$)$_2$ has been successfully prepared. This particular stoichiometry was targeted as a candidate solid-state proton conductor because of its anticipated structural similarity to known M$_3$H(XO$_4$)$_2$ superprotonic conductors (M = Cs, Rb, NH$_4$, K; X = Se, S)[1] and to the known trigonal compound Ba$_3$(PO$_4$)$_2$.[2] The materials were synthesized from aqueous solution using barium acetate, dipotassium hydrogen phosphate, and potassium hydroxide as starting materials. Through variations in the initial solution stoichiometry or the synthesis temperature, the final stoichiometry could be controlled from $x \sim 0.5$ to ~1. X-ray powder diffraction, energy dispersive spectroscopy chemical analysis, ^{1}H magic angle spinning (MAS) nuclear magnetic spectroscopy, and thermogravimetric analysis were all employed to establish potassium and proton incorporation. The diffraction data confirmed crystallization of a trigonal phase, and chemical analysis showed the (Ba+K):P ratio to be 3:2, consistent with the target stoichiometry. The conductivity of the Ba$_{3-x}$K$_x$H$_x$(PO$_4$)$_2$ materials, as measured by A.C. impedance spectroscopy, is about 3 orders of magnitude greater than the end-member Ba$_3$(PO$_4$)$_2$ material with only a slight dependence on x, however, it is substantially lower than that of typical superprotonic conductors and of the M$_3$H(XO$_4$)$_2$ materials in particular. The close proximity of Ba to the hydrogen bond site is proposed to explain this behavior. At 250 °C, the conductivity is $\sim 2.4 \times 10^{-5}$ S/cm for the composition $x = 0.80$, which, when combined with the water insolubility and the relatively high thermal stability, may render Ba$_{3-x}$K$_x$H$_x$(PO$_4$)$_2$ an attractive alternative in selected electrochemical applications to known superprotonic conductors.

Introduction

Solid acids, or acid salts, are a class of proton conducting electrolytes with stoichiometries MHXO$_4$, M$_3$H(XO$_4$)$_2$ (M = Cs, Rb, NH$_4$; M = S, Se), and MH$_2$X′O$_4$ (X′ = P, As).[3] Many of these compounds undergo a remarkable phase transition at which the proton conductivity jumps by 3−4 orders of magnitude to a "superprotonic" state with conductivity in the range of $10^{-3}-10^{-1}\,\Omega^{-1}\,\mathrm{cm}^{-1}$.[4−7] These high levels of conductivity are a result of rapid tetrahedral librations in combination with a high rate of proton transfer between tetrahedral groups.[8−10] The proton transport process is an example of the Grotthuss mechanism, in which proton migration occurs via dipole (in this case, H$_n$XO$_4^{n-2}$ or H$_n$XO$_4^{n-3}$) reorientation, structural relaxation, and proton hopping.[8]

The solid nature of superprotonic solid acids renders them inherently advantageous for a variety of electrochemical applications relative to liquid or even polymeric proton-conducting counterparts in that the need to confine the electrolyte and ensure compatibility with confinement materials is immediately eliminated. Moreover, solid acid electrolytes operate in a temperature range, 100−300 °C, that is highly desirable with respect to catalytic activity, catalyst impurity tolerance, overall thermal management, and material and thermal compatibility.[11] In recognition of these advantages, several laboratories have now demonstrated the feasibility of solid acid fuel cells.[12−17] The highest power outputs to date,

[†] Accepted as part of the 2010 "Materials Chemistry of Energy Conversion Special Issue".
*Corresponding author. E-mail: calum@caltech.edu.
(1) Bohn, A.; Melzer, R.; Sonntag, R.; Lechner, R. E.; Schuck, G.; Langer, K. *Solid State Ionics* **1995**, *77*, 111–117.
(2) Sugiyama, K.; Tokonami, M. *Mineral. J.* **1990**, *15*, 141–146.
(3) Haile, S. M.; Boysen, D. A.; Chisholm, C. R. I.; Merle, R. B. *Nature* **2001**, *410*(6831), 910–913.
(4) Pawlowski, A.; Pawlaczyk, Cz.; Hilzcer, B. *Solid State Ionics* **1990**, *44*, 17–19.
(5) Ramasastry, C.; Ramaiah, A. S. *J. Mater. Sci. Lett.* **1981**, *16*, 2011–2016.
(6) Baranov, A. I.; Khiznichenko, V. P.; Shuvalov, L. A. *Ferroelectrics* **1989**, *100*, 135–141.
(7) Baranov, A. I.; Shuvalov, L. A.; Shchagina, N. M. *JETP Lett.* **1982**, *36*(11), 459–462.
(8) Kreuer, K. D.; Dippel, T.; Hainovsky, N. G.; Maier, J. *Phys. Chem. Chem. Phys.* **1992**, *96*(11), 1736–1742.
(9) Badot, J. C.; Colomban, P. *Solid State Ionics* **1989**, *35*(1−2), 143–149.
(10) Wood, B. C.; Marzari, N. *Phys. Rev. B* **2007**, *76*(13).

(11) Norby, T. *Solid State Ionics* **1999**, *125*(1−4), 1–11.
(12) Otomo, J.; Tamaki, T.; Nishida, S.; Wang, S. Q.; Ogura, M.; Kobayashi, T.; Wen, C. J.; Nagamoto, H.; Takahashi, H. *J. Appl. Electrochem.* **2005**, *35*(9), 865–870.
(13) Uda, T.; Haile, S. M. *Electrochem. Solid-State Lett.* **2005**, *8*(5), A245–A246.
(14) Boysen, D. A.; Uda, T.; Chisholm, C. R. I.; Haile, S. M. *Science* **2004**, *303*(5654), 68–70.
(15) Bocchetta, P.; Ferraro, R.; Di Quarto, F. *J. Power Sources* **2009**, *187*(1), 49–56.
(16) Yoshimi, S.; Matsui, T.; Kikuchi, R.; Eguchi, K. *J. Power Sources* **2008**, *179*(2), 497–503.
(17) Uda, T.; Boysen, D. A.; Chisholm, C. R. I.; Haile, S. M. *Electrochem. Solid-State Lett.* **2006**, *9*(6), A261–A264.

exceeding 0.6 W/cm^2 peak power, have been obtained using CsH$_2$PO$_4$ as the electrolyte in electrode supported, thin-membrane configurations.[13,18]

While fuel-cell viability has been demonstrated using CsH$_2$PO$_4$ and CsHSO$_4$, the physical characteristics of these and other known solid acids introduce system level challenges that would ideally be addressed through the discovery of new materials. For example, acid sulfate and selenates are unstable with respect to reduction under H$_2$ in the presence of typical fuel cell anode catalysts[19,20] and as such are entirely unsuitable for realistic fuel cell applications. Eliminating these compounds leaves only phosphates and possibly arsenates among known superprotonic conductors. However, many of the compounds within this subset have rather high superprotonic transition temperatures (e.g., 228 °C for CsH$_2$PO$_4$[21] and 256 °C for Rb$_{0.75}$Cs$_{0.25}$H$_2$PO$_4$[22]) above which dehydration can also occur.[21,23,24] Consequently, device operation in the superprotonic regime necessitates application of relatively high water partial pressures (0.3−0.5 atm), a requirement that, in turn, lowers fuel cell efficiency.[18] Moreover, all known superprotonic conductors are decidedly water-soluble, and care is required to prevent condensation of liquid water from the highly humidified atmosphere onto the electrolyte. An additional complication surrounds the possibility of mechanical failure of the membrane due to the rather large volume change on heating through the superprotonic transition (for example 0.5% for CsHSO$_4$[20] and 1.7% for CsH$_2$PO$_4$[22]). The enormous potential of truly solid electrolytes for advancing electrochemical energy conversion technologies motivates a search for materials that display the high proton conductivity of known superprotonic conductors but are free of these limitations. This work is aimed precisely toward such a goal: the development of water-insoluble superprotonic conductors of high chemical and thermal stability over a large temperature range, and displaying small to no transition volume change upon reaching the temperature of operation.

The materials discovery approach taken here relies on the recognition of the structural similarities between two classes of compounds: M$_3$H(XO$_4$)$_2$ superprotonic conductors, where M = K, Rb, NH$_4$, Cs and X = Se,[1,25] and M′$_3$(X′O$_4$)$_2$ paraelectrics, where M′ = Ba, Sr, Pb, and X′ = P, As, V.[26−28]

In the superprotonic state, the M$_3$H(XO$_4$)$_2$ alkali metal compounds adopt a trigonal structure that is essentially identical to that of the M′$_3$(X′O$_4$)$_2$ alkaline earth metal compounds in their high-temperature, paraelectric state. At reduced temperatures, the transition in both classes is to a monoclinic phase that constitutes a slight distortion to the higher symmetry parent structure. Remarkably, the presence of the proton in the alkali metal compounds has little influence on the overall arrangement of metal cations and oxyanion groups relative to the alkaline earth compounds. In the trigonal phase of the alkali metal phase oxyanion group reorientation occurs about the 3-fold axis of symmetry (see discussion of structure below), facilitating proton transfer, and a similar type of disorder has been suggested in the alkaline compounds, irrespective of the absence of hydrogen bonds. Furthermore, the specific composition Ba$_3$(PO$_4$)$_2$ retains the nominally high-temperature trigonal form at all accessible low temperatures.[29] These characteristics suggest that compounds in which some portion of the Ba in Ba$_3$(PO$_4$)$_2$ has been replaced with a combination of an alkali metal, specifically, K, because of its similar size to Ba, and a proton can be synthesized, that such compounds will display high, if not superprotonic, conductivity, and that they will exhibit such behavior over a temperature range spanning from below ambient to values typical of dehydration in other superprotonic compounds (well over 200 °C). Moreover, the water insolubility of both Ba$_3$(PO$_4$)$_2$ and the related solid acid BaHPO$_4$[30] suggests that compounds with the hypothesized stoichiometry, Ba$_{3−x}$K$_x$H$_x$(PO$_4$)$_2$,will additionally display a high degree of insolubility in water.

It is noteworthy that a somewhat related approach has been suggested by Baranov et al., who have attempted to prepare alkali metal doped Ba$_3$(PO$_4$)$_2$ and subsequently inject protons at high temperature by annealing in humidified atmospheres.[31] Such a doping strategy requires condensation and subsequent hydrolysis of phosphate groups, limiting its crystal-chemical flexibility, and indeed success has yet to be convincingly demonstrated. In the present study, we pursue a direct synthesis approach and provide evidence from a range of analytical techniques that the desired stoichiometry has been achieved, and we further demonstrate the role of proton incorporation on conductivity.

Experimental Procedures

Synthesis. Synthesis of the Ba$_{3−x}$K$_x$H$_x$(PO$_4$)$_2$ compounds was achieved by a route analogous to that reported for the preparation of K$_3$CaH(PO$_4$)$_2$ in which an aqueous solution of the alkaline earth acetate is mixed with another solution of potassium hydroxide and excess dipotassium hydrogen phosphate.[32] Starting materials here were Ba(CH$_3$COO)$_2$ (99%, Alpha Aesar, #A10316), K$_2$HPO$_4$ (98%, Alpha Aesar,

(18) Chisholm, C. R. I.; Boysen, D. A.; Papandrew, A. B.; Zecevic, S.; Cha, S.; Sasaki, K.; Varga, A.; Giapis, K. P.; Haile, S. M. *Interface Mag*. **2009**, *18*(3), 53−59.
(19) Merle, R. B.; Chisholm, C. R. I.; Boysen, D. A.; Haile, S. M. *Energy Fuels* **2003**, *17*(1), 210−215.
(20) Uda, T.; Boysen, D. A.; Haile, S. M. *Solid State Ionics* **2005**, *176* (1−2), 127−133.
(21) Haile, S. M.; Chisholm, C. R. I.; Sasaki, K.; Boysen, D. A.; Uda, T. *Faraday Discuss*. **2007**, *134*, 17−39.
(22) Louie, M. W. ; Kislitsyn, M.; Bhattacharya, K.; Haile, S. M. Solid State Ionics, in press.
(23) Taninouchi, Y.; Uda, T.; Awakura, Y. *Solid State Ionics* **2008**, *178* (31−32), 1648–1653.
(24) Taninouchi, Y. K.; Uda, T.; Awakura, Y.; Ikeda, A.; Haile, S. M. *J. Mater. Chem.* **2007**, *17*(30), 3182–3189.
(25) Sonntag, R.; Melzer, R.; Knight, K. S.; Radaelli, P. G. *Mater. Sci. Forum* **1998**, *278−2*, 726−731.
(26) Zachariasen, W. H. *Acta Crystallogr.* **1948**, *1*(1−6), 263−265.
(27) Park, C. H.; Bluhm, K. *J. Chem. Sci.* **1996**, *51*(5), 722−726.
(28) Susse, P.; Buerger, M. J. *Z. Kristallogr.* **1970**, *131*(3), 161−174.
(29) Salje, E.; Bismayer, U.; Wruck, B.; Hensler, J. *Phase Transitions* **1991**, *35*(2), 61−74.
(30) Pan, D. Y.; Yuan, D. R.; Sun, H. Q.; Guo, S. Y.; Wang, X. Q.; Duan, X. L.; Luan, C. N.; Li, Z. F. *Cryst. Res. Technol.* **2006**, *41*(3), 236–238.
(31) Baranov, A. I.; Duda, V. M.; Jones, D. J.; Roziere, J.; Sinitsyn, V. V.; Slade, R. C. T. *Solid State Ionics* **2001**, *145*(1−4), 241–247.
(32) Frazier, A. W.; Smith, J. P.; Brown, W. E.; Lehr, J. R. *Inorg. Chem.* **1962**, *1*(4), 949–951.

Table 1. Synthesis Parameters for $Ba_{3-x}K_xH_x(PO_4)_2$ Compounds

synthesis no.	parameter varied	$T_{solutions}$ (°C)	K_2HPO_4 (M)
1	K concentration	23	3.6
2	K concentration	23	7.3
3	default	23	14.6
4	temperature	20	14.6
5	temperature	25	14.6
6	temperature	30	14.6
7	temperature	40	14.6
8^a	temperature	90	14.6

^{a} Stirred for only 1 min after initial mixing; all other solutions stirred for 10 min.

#11593), KOH (89%, Mallinckrodt Chemicals, #6984−04), and deionized water. The molar concentration of the barium acetate solution was fixed at 0.3 M. In the potassium bearing solution, the potassium hydroxide concentration was fixed at 0.4 M, whereas that of the dipotassium hydrogen phosphate was varied, being either 3.6, 7.3, or 14.6 M. In addition to K_2HPO_4 concentration, the impact of temperature (20−90 °C) on the final product stoichiometry was explored. For a typical synthesis 12.5 mL of the barium acetate solution was added to 36 mL of the potassium bearing solution under vigorous stirring to ensure rapid mixing of the reagents. The combined solution was stirred for an additional 10 min beyond the initial contact to ensure complete reaction of reagents. The resulting crystallites were collected on a ceramic filter, washed several times with water, then once with acetone, and subsequently dried at 75 °C. Significant synthesis parameters are summarized in Table 1. For experimental convenience, smaller quantities of material were produced by varying solution stoichiometry and selected characterization methods were restricted to materials produced by varying the solution temperature.

For comparative purposes, the end-member $Ba_3(PO_4)_2$ was synthesized by solid state reaction starting with stoichiometric amounts of $BaCO_3$ (99%, Alpha Aesar, #A10316) and $NH_4H_2PO_4$ (98%, Alpha Aesar, #A15283) mechanically milled together with a mortar and pestle for 10 min. The mixture was then placed into a alumina crucible, heated to 1200 °C at a heating rate of 5 °C/min in ambient air, held at 1200 °C for 2 h, and then cooled to room temperature at 20 °C/min (i.e., as fast as furnace would cool). The resulting powder was then ground for 5 min to break up agglomerates.

Characterization. The resulting compounds were characterized by several methods to establish the phase and stoichiometry obtained from the syntheses. Crystal morphology evaluation and chemical analysis were performed with a LEO 1550 VP field emission scanning electron microscope (SEM) equipped with an Oxford INCA Energy 300 X-ray energy dispersive spectrometer (EDS) system, where the chemical analysis was carried out on pressed pellet samples (prepared as below). The materials were carbon coated to avoid charging. X-ray powder diffraction patterns were collected from ground powder samples using a Philips PW3040-Pro diffractometer with Cu Kα radiation. Crystal structure refinement using the diffraction data was performed with Philips X'Pert Plus (Version 1.0) software. Magic angle spinning (MAS) proton nuclear magnetic resonance (NMR) measurements were performed on compressed powder samples using a Bruker DSX 500 spectrometer with a spinning rate of 12 kHz. A 4 μs, 90° pulse was employed along with a delay time of 1000 s to allow nearly complete spin−lattice relaxation and thereby obtain full peak intensities. The measured chemical shifts are referenced to tetramethylsilane. For comparative purposes, spectra were collected additionally from
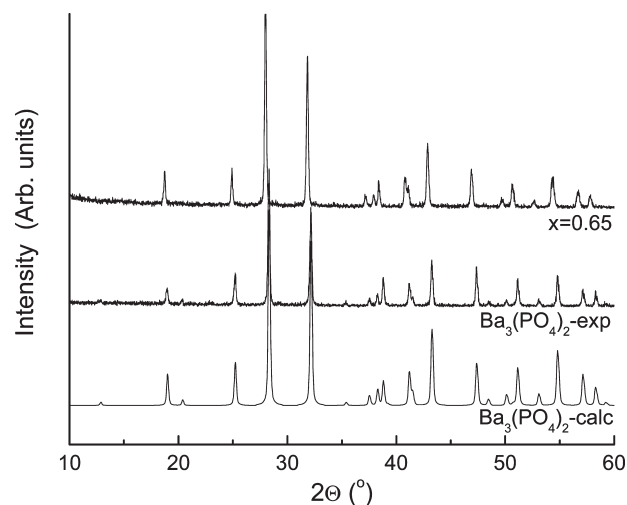

Figure 1. Comparison of a representative, measured X-ray powder diffraction pattern of $Ba_{3-x}K_xH_x(PO_4)_2$, synthesis no. 3, with the measured and calculated patterns of $Ba_3(PO_4)_2$, the latter based on the structure reported by Sugiyama and Tokonami.[2]

$K_3H(SO_4)_2$, prepared as described elsewhere.[33] Thermal gravimetric analysis (TGA) was performed on loose powder with a Netzsch STA 449 under flowing oxygen (50 cm^3/min) with a nitrogen purge (50 cm^3/min). Conductivity of pressed pellet samples was measured using A.C. impedance spectroscopy. Silver paint (Ted Pella, #16032) was applied as electrodes, and impedance data were collected using a HP 4284A LCR meter. The applied voltage was 0.75 V, and the frequency range 20 Hz to 1 MHz. Pellets were formed in a 11 mm diameter die using 60 000 psi for 5 min, with a final pellet thickness of around 1 mm. All samples, including the end-member $Ba_3(PO_4)_2$ were examined without additional sintering and accordingly displayed moderate densities, 60−80% of theoretical. The D.C. conductivity was evaluated from the frequency dependent data using an equivalent circuit model comprised simply of a resistor in parallel with a constant phase element. Data analysis was performed using the commercial software package ZView.[34]

Results and Discussion

The synthesis yielded crystallites, 0.2−2 μm in size, of trigonal and occasionally hexagonal morphology, consistent with the anticipated $R3\overline{m}$ crystalline symmetry. The X-ray diffraction patterns, a representative example of which is presented in Figure 1, indicated that the synthesized materials are structurally almost identical to the parent $Ba_3(PO_4)_2$ phase, but with a slight increase in cell constant, consistent with the substitution of a portion of the Ba^{2+} with the larger radius ion, K^+.[35] The EDS chemical analysis, Table 2, showed not only significant potassium incorporation in all samples, but also that the $(Ba+K):P$ ratios are all close to the ideal value of 1.5:1 for a general stoichiometry of $Ba_{3-x}K_xH_x(PO_4)_2$. As might be expected, increasing the K_2HPO_4 content in the solution caused a measurable but small increase in the potassium content in the final product. Specifically, the value of

(33) Chisholm, C. R. I.; Haile, S. M. *Solid State Ionics* **2001**, *145*(1−4), 179–184.
(34) *ZView Version 2.3f*; Scribner Associates: Southern Pines, NC, 2001.
(35) Shannon, R. D.; Prewitt, C. T. Acta Crystallogr., Sect. B: Struct. Crystallogr. Cryst. Chem. **1970**, *B 26*, 1046−1048.

Table 2. Results of EDS Chemical Analysis of $Ba_{3-x}K_xH_x(PO_4)_2$ Compounds

synthesis no.	K^a	Ba^a	P^a	(K+Ba):P	x^b
1	0.44 ± 0.02	2.20 ± 0.02	1.78 ± 0.01	1.48 ± 0.02	0.48 ± 0.02
2	0.50 ± 0.02	2.31 ± 0.02	2.04 ± 0.02	1.38 ± 0.02	0.55 ± 0.02
3	0.60 ± 0.03	2.20 ± 0.02	2.05 ± 0.03	1.38 ± 0.03	0.65 ± 0.02
4	0.53 ± 0.02	2.40 ± 0.03	1.97 ± 0.02	1.49 ± 0.05	0.55 ± 0.02
5	0.74 ± 0.02	2.20 ± 0.02	2.00 ± 0.02	1.43 ± 0.03	0.75 ± 0.02
6	0.78 ± 0.03	2.12 ± 0.02	2.03 ± 0.02	1.42 ± 0.04	0.80 ± 0.03
7	0.76 ± 0.02	1.79 ± 0.08	1.76 ± 0.03	1.45 ± 0.08	0.89 ± 0.02
8	0.96 ± 0.03	2.02 ± 0.03	2.01 ± 0.02	1.49 ± 0.04	0.97 ± 0.03

^{a} Absolute stoichiometric content. ^{b} Normalized potassium content such that stoichiometric contents of K, Ba, and P sum to 5.
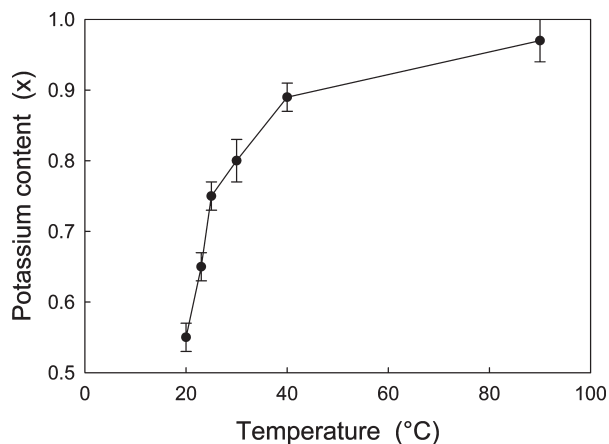

Figure 2. Potassium incorporation in $Ba_{3-x}K_xH_x(PO_4)_2$ as a function of synthesis temperature, as determined by EDS chemical analysis (conditions 3−8 of Table 1).

x could be increased from 0.48 to 0.65 by tripling the K_2HPO_4 content. A stronger influence on stoichiometry was solution temperature, Figure 2. For a given K_2HPO_4 content, increasing the solution temperature from 20 to 90 °C increased x from 0.55 to 0.97, and, in the lower end of the explored temperature range, the sensitivity to temperature is rather high. The highest potassium content obtained ($x = 0.97$) implies a stoichiometry of approximately $Ba_2KH(PO_4)_2$, which is the precise chemical analog to $Rb_3H(SeO_4)_2$, with one proton for every two tetrahedral groups. At this stage it is unknown whether $x = 1$ is, in fact, the maximum K content that can be incorporated into $Ba_{3-x}K_xH_x(PO_4)_2$ or if further adjustments to the synthesis conditions might yield $x > 1$. The trend evident in Figure 2, however, suggests that simply increasing temperature is unlikely to result in higher potassium concentrations.

Rietveld refinement of the $Ba_{3-x}K_xH_x(PO_4)_2$ structures were performed to directly evaluate from the X-ray data the extent of potassium incorporation and to quantify the variation in cell constant with potassium content. The known structure of $Ba_3(PO_4)_2$ was used as a starting point for these refinements, Table 3,[2] and the potassium introduced equally onto both crystallographically distinct Ba atom sites of the structure. The occupancies were refined with the constraint that each site be fully occupied, but the relative K and Ba occupancies were otherwise allowed to vary freely. All variable atomic coordinates were held fixed to the values reported for $Ba_3(PO_4)_2$, consistent with the fact that the free coordinates in

$Ba_3(PO_4)_2$ and $Rb_3(SeO_4)_2$ are almost identical to one another, Table 3.

The results of the Rietveld analysis are summarized in Table 4 and Figures 3 and 4. The cell volume, Figure 3(a), varies linearly with potassium content (the latter being that obtained from the EDS chemical analysis) and follows almost precisely what one expects based on the relative sizes of the potassium and barium ions,[35] shown as a solid line in the figure. Moreover, the potassium content obtained from the Rietveld refinement matches, within error, the results of the EDS chemical analysis, Figure 3(b), further confirming that potassium has been successfully incorporated in the compound.

Turning to the details of the structural implications of potassium incorporation, a rather surprising observation, Figure 4(a), is that the potassium is preferentially situated at the M(2) site, being almost entirely excluded from the M(1) site. Furthermore, Figure 4(b), whereas the a lattice constant increases almost linearly with x (including extrapolation down to $x = 0$), the c lattice constant displays a sharp initial increase from its value in $Ba_3(PO_4)_2$ with relatively small amounts of potassium incorporation, then rises only slightly before decreasing for $x > 0.75$. As shown in the structural depictions of Figure 5, the structure of $Ba_3(PO_4)_2$ (and, by definition of the refinement procedure, that of $Ba_{3-x}K_xH_x(PO_4)_2$ also) is composed of layers of phosphate tetrahedra, within which the PO_4 groups all point in the same direction and are arranged in a trigonal array. These layers are further arranged in pairs (or double layers) along $\langle 001 \rangle$ with apical O(1) oxygen atoms directed toward the other layer of the pair, but with phosphate groups offset from each other along $\langle \bar{1}10 \rangle$. This arrangement creates what appears in projection along $\langle 001 \rangle$ as a hexagonal net of phosphate groups, with the M(1) cations residing at the center of each the apparent hexagons, Figure 5(a). The M(2) cations form double layers with an arrangement identical to that of the phosphate double layers, and the overall structure is built up by stacking alternating M(2) and PO_4 double layers along $\langle 001 \rangle$, Figure 5(b). The coordination polyhedra about M(1) are formed of six O(2) and six O(1) atoms with, in the case of $Ba_3(PO_4)_2$, Ba−O bond distances of 2.737(2) and 3.2354(3) Å, respectively. The M(2) cation is coordinated by 10 oxygen atoms, one O(1), six O(2) and three O(1) with bond distances (again, in the specific case of $Ba_3(PO_4)_2$) of 2.636(8), 2.858(1), and 2.906(2) Å, respectively. The preference of the potassium for the M(2) site can be understood in terms of the differences

Table 3. Crystallographic Parameters of Ba₃(PO₄)₂ (a = 5.6038(7) and c = 21.000(5) Å) and Rb₃H(SeO₄)₂ (a = 6.1291(1) and c = 22.656(5) Å) in Space Group R3̄m:H[a]

		Ba₃(PO₄)₂[2]				Rb₃H(SeO₄)₂[1]		
	site	x/a	y/b	z/c	site	x/a	y/b	z/c
M(1)	3a	0	0	0	3a	0	0	0
M(2)	6c	0	0	0.20860(2)	6c	0	0	0.2024(6)
X	6c	0	0	0.4075(1)	6c	0	0	0.4092(5)
O(1)	6c	0	0	0.3341(3)	18 h[b]	0.046(1)	−0.046(1)	0.338(1)
O(2)	18 h	0.1502(4)	−0.1502(4)	0.5676(2)	18 h	0.1450(3)	−0.1450(3)	0.5711(5)
H	n/a				18 h[c]	0.452(3)	0.548(3)	0.000(4)

[a] Number in parentheses indicates uncertainty in final digit. [b] Occupancy of 1/3 and slightly displaced from average position on 6c site at 0, 0, 0.338. [c] Occupancy of 1/6 and slightly displaced from average position on 9e site at 0.5, 0.5, 0.

Table 4. Results of X-ray Reitveld Refinement of Ba₃₋ₓKₓHₓ(PO₄)₂ Structures[a]

synthesis no.	R_{Bragg}	vol. (Å³)	a (Å)	c (Å)	x_{Total}	$x_{M(1)}$	$x_{M(2)}$
1	7.21	577.8(2)	5.6209(5)	21.114(2)	0.51(6)	0.05(2)	0.23(2)
2	6.94	579.0(2)	5.6266(5)	21.120(2)	0.59(6)	0.04(2)	0.27(2)
3	7.84	580.0(1)	5.6304(4)	21.128(2)	0.70(6)	0.06(2)	0.32(2)
4	4.97	578.3(1)	5.6211(2)	21.136(1)	0.58(4)	0.06(2)	0.26(1)
5	5.18	581.8(1)	5.6359(2)	21.151(1)	0.80(6)	0.08(2)	0.36(2)
6	5.16	582.8(2)	5.6421(5)	21.139(2)	0.85(4)	0.07(2)	0.39(1)
7	4.25	584.8(1)	5.6532(3)	21.130(1)	0.94(6)	0.08(2)	0.43(2)
8	4.47	586.5(1)	5.6640(4)	21.110(1)	1.01(5)	0.13(1)	0.44(2)

[a] Number in parentheses indicates uncertainty in final digit.

Table 5. Results of Thermogravimetric Measurement of Water Content in Ba₃₋ₓKₓHₓ(PO₄)₂[a]

synthesis	TGA wt loss (%)	x−apparent TGA wt loss	$I_{bulk}/I_{surface}$ −H[1] NMR	x−bulk TGA wt loss
4	1.30	0.792 ± 0.006	2.21 ± 0.06	0.55 ± 0.05
5	1.72	1.01 ± 0.01	2.83 ± 0.04	0.75 ± 0.05
6	1.82	1.058 ± 0.006	3.04 ± 0.03	0.80 ± 0.03
7	1.88	1.076 ± 0.006	4.93 ± 0.03	0.89 ± 0.03
8	1.82	1.026 ± 0.006	15.8 ± 0.1	0.96 ± 0.03

[a] By making use of the ¹H NMR data it is possible to differentiate between surface sorbed and bulk, crystallographic water. Specifically, the apparent proton content obtained from the total weight loss is modified by the relative bulk proton concentration obtained from the ratio of the 12.5 and 6.5 ppm NMR peak intensities (4th column) to yield the true bulk proton concentration (final column).

in the local coordination geometries. In the M(2) site, elongation of a single bond, to the first O(1) atom, provides much of the structural relaxation required to accommodate the larger potassium ion. This M(2)−O(1) bond is directed exactly along ⟨001⟩ and hence potassium incorporation induces an immediate, large increase in c relative to the increase in a. Further introduction of potassium expands the lattice along a, but the initial expansion along c to accommodate even small amounts of potassium apparently results in an M(2) coordination polyhedron that does not require further increases in the short M(2)−O(1) bond. The reason for the decrease in c at very high potassium content is not immediately obvious, but it is possible to speculate that this behavior reflects a displacement of the O(1) oxygen atom from the triad axis, from the 6c site to an 18 h site, as is the case in the high-temperature form of Rb₃H(SeO₄)₂, Table 3.[1] With such a displacement, the M(2)−O(1) bonds may plausibly remain long while the c axis contracts.

Whereas the EDS chemical analysis and X-ray powder diffraction results clearly demonstrate the incorporation

of potassium into the product compound, they do not directly reveal the presence of hydrogen. For direct confirmation, it is appropriate to turn to the NMR studies. The ¹H NMR spectra, Figure 6, demonstrate that protons are indeed present in the Ba₃₋ₓKₓHₓ(PO₄)₂ compounds. The spectra show one broad peak at a shift of approximately 12.5 ppm and a second, slightly sharper peak at approximately 6.5 ppm. In general, the features of the 6.5 ppm peak varied erratically from sample to sample (including integrated intensity, peak breadth, and position), whereas those of the 12.5 ppm displayed relatively systematic behavior. Both the trigonal and monoclinic phases of the M₃H(XO₄)₂ class of compounds have only one crystallographic proton site (the latter being a slight distortion of the former), and hence only one peak is expected in the ¹H NMR spectrum for an isostructural material. In the case of monoclinic K₃H(SO₄)₂, our measurement reveals a single sharp peak at 16.4 ppm, and similarly, a single sharp peak at 16.3 ppm has been observed in monoclinic Rb₃H(SO₄)₂.[36] Peaks of lower chemical shift, in the 5−8 ppm range, and with less reproducible behavior are typical of chemisorbed H₂O on solid acids.[37−39] These observations suggest that the peak at 12.5 ppm in Ba₃₋ₓKₓHₓ(PO₄)₂ corresponds to structurally incorporated protons and that at 6.3 ppm peak to surface species. Heat treatment at 200 °C under vacuum caused a reduction in the 6.3 ppm peak intensity but had no impact on the 12.5 ppm peak (not shown), further supporting the conclusion that the former peak is

(36) Suzuki, K.; Hayashi, S. *Phys. Rev. B* **2006**, *73*(2), 024305.
(37) Boysen, D. A.; Haile, S. M.; Liu, H. J.; Secco, R. A. *Chem. Mater.* **2003**, *15*(3), 727–736.
(38) Cowan, L. A. Ph.D. Dissertation, California Institute of Technology, **2007**.
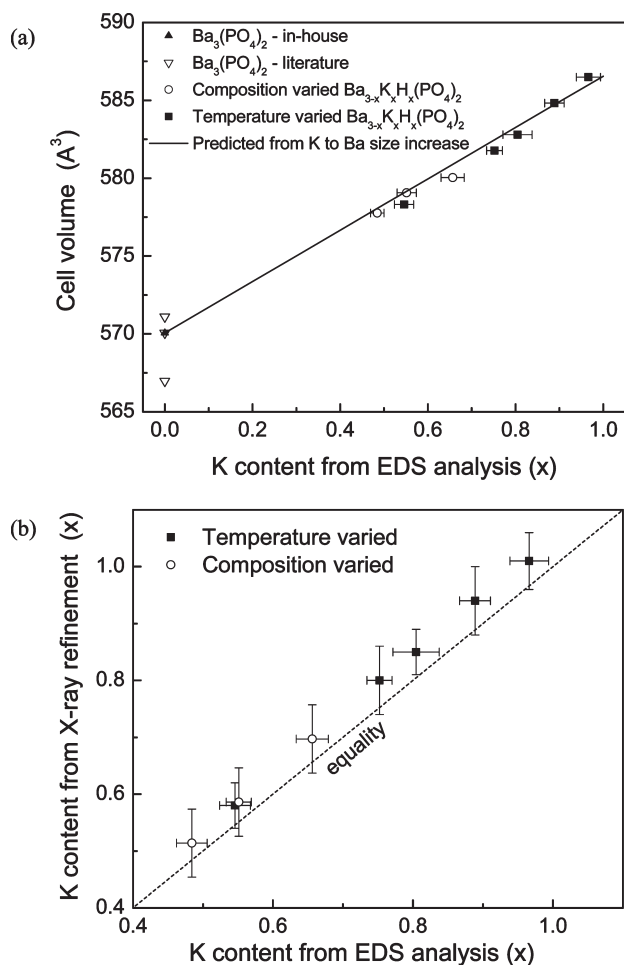(39) Kislitsyn, M. Ph.D. Dissertaion, California Institute of Technology, **2009**.

Article

Chem. Mater., Vol. 22, No. 3, 2010 1191

Figure 3. Selected results from Rietveld analysis of $Ba_{3-x}K_xH_x(PO_4)_2$ X-ray powder diffraction data: (a) increase in cell volume with potassium content, x, shown in comparison to the predicted cell constant on the basis of the radius of K^+; and (b) refined potassium content versus EDS measured potassium content. As indicated, closed symbols are for temperature varied synthesis experiments and open for composition varied experiments.

Figure 4. Selected results from Rietveld analysis of $Ba_{3-x}K_xH_x(PO_4)_2$ X-ray powder diffraction data: (a) refined K occupancy in the two distinct cation sites, M(1) and M(2), as a function of potassium content as determined from EDS analysis; and (b) K content, x, from EDS data versus refined a and c lattice constants. Closed symbols are for temperature varied synthesis experiments and open for composition varied. In (b) solid lines are guides to the eye, dotted lines indicate reported cell constants for $Ba_3(PO_4)_2$.[2]

due to a surface sorbed species. Residual acid on the particle surfaces, however, is unexpected because of the highly basic conditions of the synthesis, leaving chemisorbed water as the most plausible candidate. The breadth of the 12.5 ppm peak in $Ba_{3-x}K_xH_x(PO_4)_2$ likely reflects the solid solution behavior and the implied variable local features of the hydrogen bond. From the value of the chemical shift for the structural proton it is possible to estimate the oxygen−oxygen distance of the hydrogen bond using the correlation between these two parameters reported by Eckert et al.[40] and obtain a value of 2.62 Å. Notably, the chemical shift appears to decrease slightly with increasing potassium concentration (from 12.9 for $x = 0.55$ to 12.3 for $x = 0.97$), suggesting a weakening of the hydrogen bond upon increasing potassium incorporation.

By analogy to the $M_3H(SeO_4)_2$ compounds, one can consider the hydrogen bonds in $Ba_{3-x}K_xH_x(PO_4)_2$ to form between apical O(1) atoms, linking the phosphate
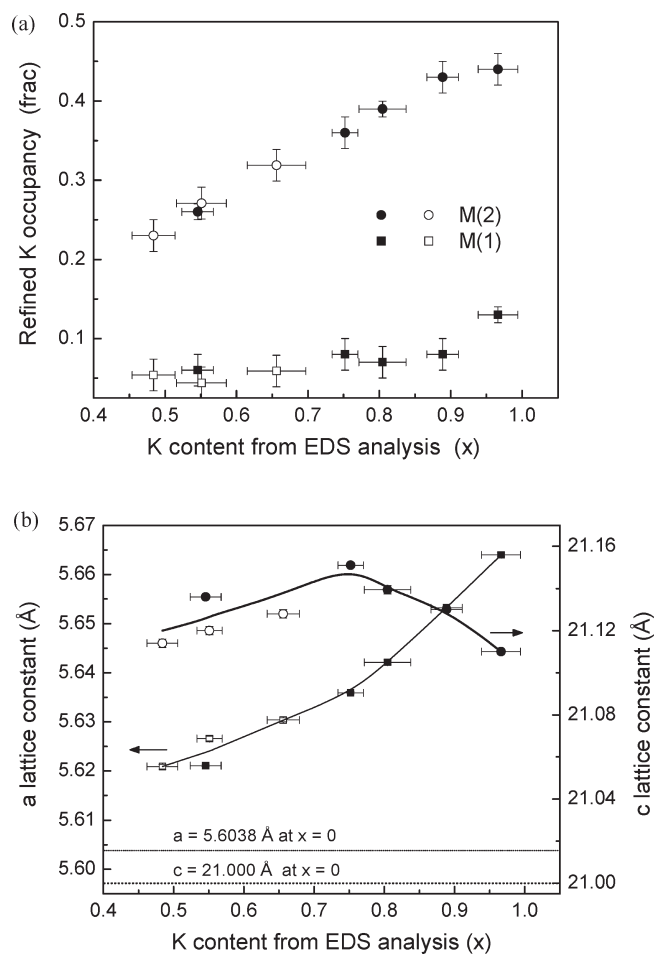
double layers. Such O(1)−O(1) linkages further form six of the twenty-four edges of the $[Ba(1)O_{12}]$ polyhedron. If the O(1) is taken to remain on the trigonal, 6c site, the relevant O(1)−O(1) distance is ∼3.24 Å, a value far too large for a meaningful hydrogen bond. Displacement of the O(1) atom from the 6c site can lead to shorter instantaneous distances in a dynamically disordered structure, as is now well-documented for the $M_3H(SeO_4)_2$ compounds. Indeed, in $Rb_3H(SeO_4)_2$ an instantaneous bond distance of 2.58(1) Å has been reported, substantially shorter than the average distance of 3.54 Å.[1] The distance from the closest cation, Ba(1), to the analogous proton location in $Ba_3(PO_4)_2$, if the proton is taken to reside precisely at the 3b site (at 0, 0, $^1/_2$), has a plausible value of 2.80 Å, and can increase slightly to a more favorable distance of ∼2.84 if again dynamic disorder occurs. Alternatively, one can, in principle, consider any one of the remaining six, crystallographically distinct Ba polyhedral edges, ranging in length from 2.53 to 3.50 Å in $Ba_3(PO_4)_2$, to serve as hydrogen bonds. However, their absence as hydrogen bonds from the selenate compounds

(40) Eckert, H.; Yesinowski, J. P.; Silver, L. A.; Stolper, E. M. *J. Phys. Chem.* **1988**, *92*(7), 2055–2064.
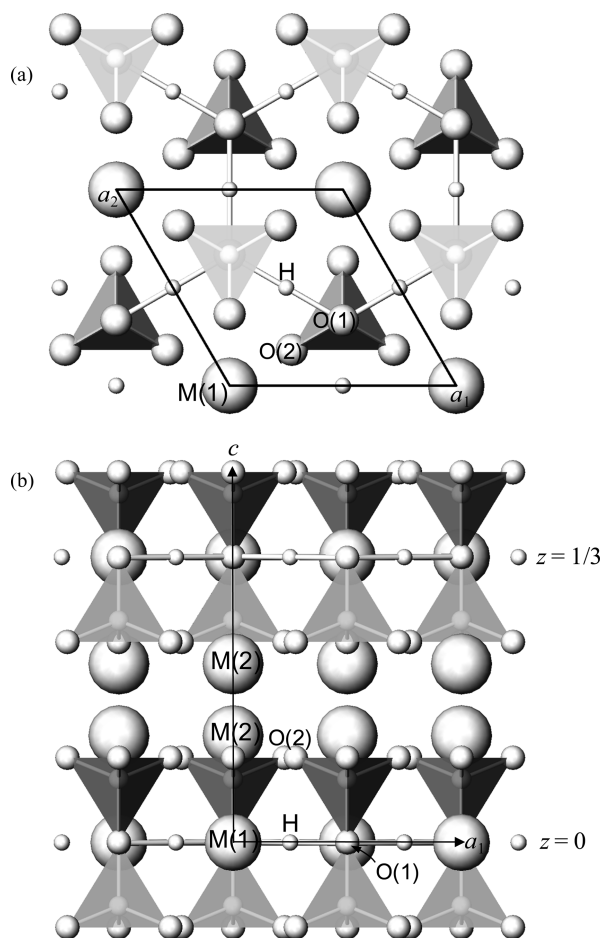
Figure 5. Structure of $Ba_{3-x}K_xH_x(PO_4)_2$ based on the known structures of $Ba_3(PO_4)_2$[2] and $Rb_3H(SeO_4)_2$.[1] (a) Projection along $\langle 001\rangle$ from just below to just above $z=0$, showing the apparent hexagonal net formed by a single, phosphate bilayer. The M(1) atoms occur at elevation $z=0$, and the idealized location of the proton is also at elevation $z=0$. The labeled O(1) and O(2) atoms occur just below $z=0$, and those of the other tetrahedral group within the unit cell occur just above $z=0$. (b) Projection on (010) (i.e., along b^*) of the cell contents from $y=-^1/_3$ to $y=1^2/_3$ and x and z as indicated, showing the stacking of two phosphate bilayers.

suggests their absence from the new phosphate prepared here. It is also of relevance that the distance between apical O(1) oxygen atoms in the proposed hydrogen bond increases monotonically with increasing potassium content, a feature reflected in the ^1H NMR chemical shifts. In contrast, some of the other oxygen−oxygen distances decrease at the highest potassium concentrations as a consequence of the anisotropic chemical expansion and decrease in c lattice constant beyond $x=0.75$, Figure 4(b). Despite the ambiguities with respect to the precise proton location in $Ba_{3-x}K_xH_x(PO_4)_2$, it is apparent that the structure contains multiple viable sites for hydrogen bond formation, with the site analogous to that in the selenate compounds being most probable.

Further evidence of proton incorporation is provided by the thermogravimetric (TG) analyses, Figure 7. The TG curves indicate a loss in weight in all compositions upon heating to 1000 °C. The process initiates between 100 and 370 °C, depending on the exact stoichiometry (with higher K content generally leading to thermal stability to higher temperatures), and is complete by approximately 900 °C.
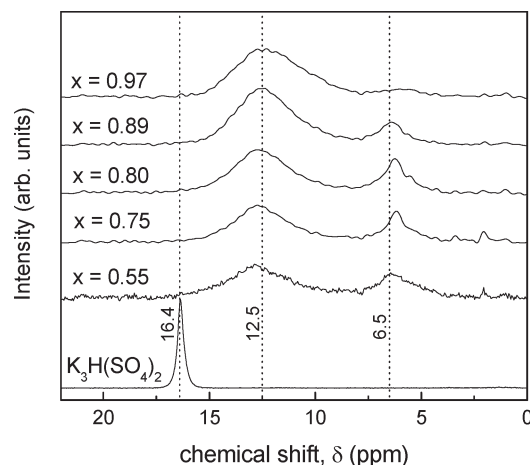

Figure 6. Mass normalized ^1H MAS NMR spectra of selected $Ba_{3-x}K_xH_x(PO_4)_2$ materials with potassium content as indicated. Measured spectrum of $K_3H(SO_4)_2$ presented for comparison. Peaks at 12.5 and 6.5 ppm are attributed, respectively, to crystalline hydrogen and chemisorbed surface water.
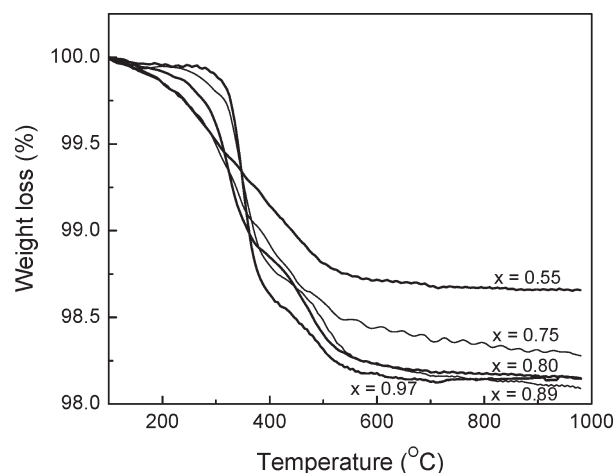

Figure 7. Thermogravimetric (TG) weight loss curves of selected $Ba_{3-x}K_xH_x(PO_4)_2$ compounds with stoichiometry as indicated, collected at a heating rate of 1 °C/min under flowing argon.

The total weight loss ranges from about 1.2 to 1.8 wt %, and increases with increasing potassium content. Examination of the product material by X-ray powder diffraction indicated complete conversion of $Ba_{3-x}K_xH_x(PO_4)_2$ to a mixture of $Ba_2P_2O_7$ and $BaKPO_4$, suggesting that the entirety of the weight change was due to dehydration, thereby enabling quantitative evaluation of the proton content. As determined from the NMR measurements, however, each $Ba_{3-x}K_xH_x(PO_4)_2$ composition contained measurable, chemisorbed surface water that would be expected to contribute to the weight loss. Thus, the structural proton content was computed under the assumption that only a given portion of the weight loss was due the structural or bulk protons, where the surface-to-bulk proton ratio was determined from the ratio of the integrated intensities of the surface and bulk NMR peaks. The results, summarized in Figure 8, show that the proton content so computed from the TG measurements match closely the values implied by the EDS chemical analysis.
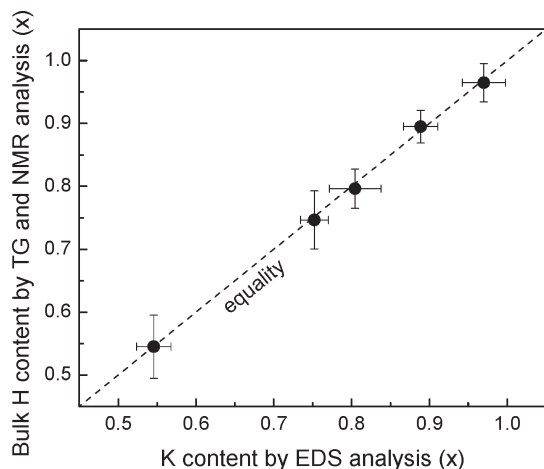
Figure 8. Comparison of x in $Ba_{3-x}K_xH_x(PO_4)_2$ measured by EDS chemical analysis of potassium content and from a combined thermogravimetric and ^{1}H NMR analysis of bulk proton content.
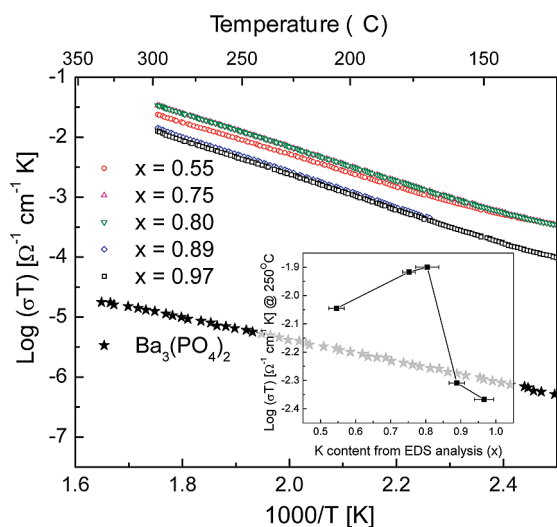

Figure 9. Conductivity of selected $Ba_{3-x}K_xH_x(PO_4)_2$ compounds with stoichiometry as indicated, collected on the second cooling cycle with a cooling rate of 1 °C/min under ambient atmospheres.

Turning to the conductivity, Figure 9, it is clear that introduction of K and H substantially increases the conductivity of $Ba_{3-x}K_xH_x(PO_4)_2$ over that of unmodified $Ba_3(PO_4)_2$, indeed, by about 3 orders of magnitude. In light of the large ionic radius of K, it is reasonable to conclude that the protons rather than the potassium ions are the mobile species, although this has not been explicitly confirmed. The activation energy for the conduction process is rather high, 0.53−0.58 eV, as compared to 0.36 eV in $Ba_3(PO_4)_2$ and values of 0.3−0.4 in typical superprotonic conductors. Somewhat surprisingly, the highest conductivity is not observed for the sample with the highest proton content. Instead, the conductivity rises and then falls with increasing x, apparently peaking at a composition of $x = 0.80$. At this stage, the detailed mechanisms behind the transport behavior are unknown. There is a temptation to attribute the trend with composition to crystal chemical features connected with the nonmonotonic chemical expansion along c, however, such a conclusion would be premature. Alternative

possibilities for this trend include changes in conductivity due to defect trapping, a common phenomenon in solid electrolytes such as zirconia and ceria subjected to an excessively high dopant concentration,[41,42] to differing amounts of residual, chemisorbed water, to differing densities, or even to differing crystallite size/morphology. The raw impedance spectra (not shown) displayed only a single electrolyte arc despite the polycrystalline nature of the materials indicating convolution between the bulk and grain boundary responses. Moreover, while the measured conductivities were generally stable over subsequent heating and cooling cycles limited to moderate temperatures of 300 °C or below, examination at higher temperatures caused slight, irreversible losses in conductivity, which could be due to either bulk or surface dehydration.

The most notable feature of the conductivity of $Ba_{3-x}K_xH_x(PO_4)_2$ is that, despite the sharp increase over undoped $Ba_3(PO_4)_2$, the value (2.4×10^{-5} S/cm at 250 °C for $x = 0.80$) is 2−3 orders of magnitude lower than that of superprotonic $Rb_3H(SeO_4)_2$ and superprotonic phases in general.[3] If one accepts that protons are incorporated into $Ba_{3-x}K_xH_x(PO_4)_2$ in a manner analogous to the selenates and sulfates, then one would, at first glance, expect comparable conductivities, particularly for $x \sim 1$. The difference may be related to the site of K incorporation in $Ba_{3-x}K_xH_x(PO_4)_2$. As noted above, the likely O(1)−O(1) hydrogen bond also forms one of the edges of the M(1) polyhedron. In the case of the selenates and sulfates, the M(1) cation is, of course, an alkali metal species, whereas in $Ba_{3-x}K_xH_x(PO_4)_2$ it is Ba^{2+}. This less polarizable cation of higher charge may impede local displacements of the oxygen atoms away from the M(1) site and toward neighboring phosphates groups, as necessary for hydrogen bond formation, simultaneously impeding the dynamic disorder required for superprotonic proton transport. It is of relevance that the nature of the disorder in the $M'_3(X'O_4)_2$ compounds is not completely known and the average $R3m$ structure may reflect static (spatial) rather than dynamic (temporal) disorder. The relatively small ^{1}H NMR chemical shifts in $Ba_{3-x}K_xH_x(PO_4)_2$ support the conclusion that the local structural distortions are insufficient to create hydrogen bonds with distances comparable to those in related solid acids. Simultaneously, the breadth of the peaks points to limited proton dynamics, as proton motion would otherwise induce peak narrowing, possibly in combination with a broad distribution of proton environments.

Summary

The aim of this work has been the rational design of new proton conducting electrolytes with attributes beyond high conductivity, including insolubility in water and chemical stability under fuel cell conditions. The targeted compound, $Ba_{3-x}K_xH_x(PO_4)$, identified from an examination of the crystal chemical features of $Ba_3(PO_4)_2$ and $Rb_3H(SeO_4)_2$, was successfully synthesized. The

(41) Fergus, J. W. *J. Power Sources* **2006**, *162*(1), 30–40.
(42) Inaba, H.; Tagawa, H. *Solid State Ionics* **1996**, *83*(1−2), 1–16.

potassium (and hence proton) content can be readily varied from $x \sim 0.5$ to ~ 1 and a wider range may be possible with additional exploration of synthesis conditions. The double substitution of potassium and of protons into the end-member phosphate dramatically increases the proton conductivity over unmodified $Ba_3(PO_4)_2$. However, the conductivity of $Ba_{3-x}K_xH_x(PO_4)_2$, which is almost independent of stoichiometry within the range of x examined, is $2-3$ orders of magnitude lower than that of superprotonic $Rb_3H(SeO_4)_2$ and of superprotonic phases in general.[3] Slight differences in the crystal chemistry of $Ba_{3-x}K_xH_x(PO_4)_2$ and superprotonic $M_3H(XO_4)_2$ may explain this difference in behavior. In particular, potassium incorporation in the former occurs in a manner that retains the Ba on the cation site close to the expected location of the hydrogen bond, and the lower polarizability of the barium relative to the alkali metals may hinder the local dynamic disorder typical of superprotonic conductivity. Further crystal chemical tailoring of the structure to alter the cation distribution and enhance the dynamic disorder may yet yield a new class of truly superprotonic acid phosphates.